Hyperon stars in the Brueckner-Bethe-Goldstone theory

M. Baldo and G. F. Burgio
Istituto Nazionale di Fisica Nucleare, Sezione di Catania and Dipartimento di Fisica, Università di Catania, Corso Italia 57, I-95129 Catania, Italy

H.-J. Schulze
Departament d'Estructura i Constituents de la Matèria, Universitat de Barcelona, Avenida Diagonal 647, E-08028 Barcelona, Spain
(Received 17 December 1999; published 13 April 2000)

In the framework of the Brueckner-Bethe-Goldstone theory, we determine a fully microscopic equation of state for asymmetric and β-stable nuclear matter containing Σ^- and Λ hyperons. We use the Paris and the new Argonne Av_{18} two-body nucleon interaction, whereas the nucleon-hyperon interaction is described by the Njimegen soft-core model. We stress the role played by the three-body nucleon interaction, which produces a strong repulsion at high densities. This enhances enormously the hyperon population, and produces a strong softening of the equation of state, which turns out almost independent on the nucleon-nucleon interaction. We use the new equation of state in order to calculate the structure of static neutron stars. We obtain a maximum mass configuration with $M_{\max}=1.26$ (1.22) when the Paris (Av_{18}) nucleon potential is adopted. Central densities are about 10 times normal nuclear matter density. Stellar rotations, treated within a perturbative approach, increase the value of the limiting mass by about 12%.

PACS number(s): 26.60.+c, 21.30.Fe, 21.65.+f, 24.10.Cn

I. INTRODUCTION

The nuclear matter equation of state (EOS) is the fundamental input for building models of neutron stars (NSs) [1]. These compact objects, among the densest ones in the universe, are produced during the gravitational collapse of massive stars, which explode into supernovae at the end of their evolution. Neutron stars are observed as pulsars: because of their fast rotation they emit only in particular directions regularly spaced pulses of electromagnetic radiation. Although almost 700 pulsars have been detected so far, their gravitational mass can be inferred only from observation of a few binary systems [2]. The observed NS masses are typically $\approx(1-2)M_\odot$ (where $M_\odot$ is the mass of the sun, $M_\odot = 1.99\times10^{33}$ g). Above $3M_\odot$, NSs are commonly believed to collapse into black holes. Typical radii of NSs are thought to be of order 10 km, although direct measurements do not exist, whereas the central density is a few times normal nuclear matter density ($\rho_0\approx0.17$ fm^{-3}). This requires a detailed knowledge of the EOS for densities $\rho\gg\rho_0$.

This is a very hard task from the theoretical point of view. For instance, the present uncertainty on the equation of state at high density implies an uncertainty on the value of the maximum mass, important for distinguishing between neutron star or a black hole formation. In fact, whereas at densities $\rho\approx\rho_0$ the matter consists mainly of nucleons and leptons, at higher densities several species of particles may appear due to the fast rise of the baryon chemical potentials with density. Among these new particles are strange baryons, namely, the Λ, Σ, and Ξ hyperons. Due to its negative charge, the Σ^- hyperon is the first strange baryon expected to appear with increasing density in the reaction $n+n\rightarrow p+\Sigma^-$, in spite of its substantially larger mass compared to the neutral Λ hyperon ($M_{\Sigma^-}=1197$ MeV, $M_\Lambda=1116$ MeV). Other species in stellar matter may appear, such as Δ isobars along with pion and kaon condensations. Moreover, at very high densities, nuclear matter is expected to undergo a transition to a quark-gluon plasma [3]. However, the exact value of the transition density is still unknown because of some technical problems in the QCD lattice calculations for finite baryon density. In this paper we disregard these phenomena, because they lie outside the scope of Brueckner theory that is applied here. In particular, we concentrate our investigation on the production of strange baryons. We assume that a baryonic description of nuclear matter holds up to densities as those encountered in the core of neutron stars.

In a previous article [4] we presented a microscopic investigation within an extended Brueckner-Hartree-Fock (BHF) scheme for determining the chemical potentials of the different baryons (n,p,Σ^-,Λ) in a fully self-consistent manner. We used in our calculations the Paris [5] and the Argonne v_{14} [6] nucleon-nucleon (NN) interaction, modified by three-body forces (TBFs), in order to get the correct saturation point of nuclear matter [7]. In that paper [4] we adopted the Nijmegen soft-core [8] potentials for describing the nucleon-hyperon interaction, whereas no hyperon-hyperon potential was taken into account, due to lack of restricting experimental data. We mainly concentrated on the calculation of the onset density of the Σ^- and Λ hyperons. We found that thresholds are reached at densities beginning at about 2–3 times normal nuclear matter density, for all the different nuclear equations of state considered.

In this paper we proceed further and present results concerning the equation of state of asymmetric and β-stable nuclear matter containing Σ^- and Λ hyperons, obtained in the BHF theoretical scheme. We adopt the Paris and the new Argonne v_{18} [9] NN potentials, eventually modified by nucleon TBFs according to the Urbana model, and the Njimegen nucleon-hyperon potentials. In these calculations still no hyperon-hyperon interaction is included. We determine microscopically the chemical potentials of the various species. Their concentration is inferred by imposing the con-

ditions of chemical equilibrium, along with charge neutrality and baryon number conservation. In general, we observe a softening of the equation of state with respect to the pure nucleonic case because of the increased number of baryonic species. The main result of our work is that in the presence of hyperons the inclusion of the nucleon TBF does not produce any significant change in the equation of state with respect to the case with only two-body forces. This is quite astonishing because, in the pure nucleon case, the repulsive character of TBFs at high density increases the stiffness of the EOS, thus changing dramatically the equation of state [7]. However, when hyperons are included, the presence of TBFs among nucleons enhances the population of Σ^- and Λ because of the increased neutron and proton chemical potentials with respect to the case without TBFs, thus decreasing the nucleon population. The net result is that the equation of state looks very similar to the case without TBFs, but the chemical composition of matter containing hyperons is very different when TBFs are included. In the latter case, the hyperon populations are larger than in the case with only two-body forces. This has very important consequences for the structure of the neutron stars. Of course, this scenario could partly change if hyperon-hyperon interactions were known or if TBFs would be included also for hyperons, but this is beyond our current knowledge of the strong interaction.

We apply our new equations of state to the calculation of the static properties of neutron stars having hyperonic cores. The values of the maximum mass configuration, i.e., mass, radius, and central density, turn out almost independent on the chosen two-body nucleon-nucleon potential. On the other hand, the values of the central densities are quite different when TBFs are taken into account, producing less compact stars than in the case without TBFs. Therefore hyperon stars, i.e., nucleon stars with hyperonic cores, collapse earlier than pure nuclear stars. Stellar rotations, which are treated here within a modified Hartle-Thorne method [10], increase the value of the maximum mass by about 12%. However, only configurations rotating at their Kepler frequency have been calculated.

This paper is organized as follows. In Sec. II we review some formalisms in the BHF scheme with hyperons, with a discussion of the method chosen for the calculation of the baryon chemical potentials. We also discuss the equilibrium compositions among the different baryonic species and the equation of state. In Sec. III we illustrate our results. In particular, in Sec. III A we discuss the behavior of the single-particle potentials for all involved species as calculated in the Brueckner theory. The matter composition is illustrated in Sec. III B, along with the equation of state. Special emphasis is put on discussing the role of the nucleonic TBFs in Sec. III C. In Sec. III D we analyze the static properties of neutron stars and their variations caused by the rotations. Our conclusions are finally drawn in Sec. IV.

II. FORMALISM

For a detailed account of the extended Brueckner theory including hyperons we refer the reader to Refs. [4] and [11]. Here we repeat only the basic formulas and give some details concerning the particular application to neutron star physics. It turns out that in this case, besides the nucleons, $N=n,p$, only the $Y=\Sigma^-,\Lambda$ hyperons appear as stable particles in the matter, limiting the baryonic Fermi seas to these four species. (Other types of hyperons appear in virtual intermediate states, of course.) We also remind the reader that for the present work no hyperon-hyperon potentials are used, leading to simplification in some places.

Then, the extended Brueckner scheme requires as input the nonrelativistic nucleon-nucleon and nucleon-hyperon potentials. With these potentials, the various G matrices are evaluated by solving numerically the Bethe-Goldstone equation [12], written schematically as

$$G_{ab}[W]=V_{ab}+\sum_c \sum_{p,p'} V_{ac}|pp'\rangle \frac{Q_c}{W-E_c+i\epsilon}\langle pp'|G_{cb}[W], \tag{1}$$

where the indices a, b, c indicate pairs of baryons and the angle-averaged Pauli operator Q and energy E determine the propagation of intermediate baryon pairs. In a given nucleon-hyperon channel $c=(NY)$ one has, for example,

$$E_{(NY)}=m_N+m_Y+\frac{k_N^2}{2m_N}+\frac{k_Y^2}{2m_Y}+U_N(k_N)+U_Y(k_Y). \tag{2}$$

The hyperon single-particle potentials within the continuous choice are given by

$$\begin{aligned} U_Y(k)&=\sum_{N=n,p} U_Y^{(N)}(k) \\ &=\mathrm{Re}\sum_{N=n,p}\sum_{k'<k_F^{(N)}} \langle kk'|G_{(NY)(NY)}[E_{(NY)}(k,k')]|kk'\rangle \end{aligned} \tag{3}$$

and similar expressions of the form

$$U_N(k)=\sum_{N'=n,p} U_N^{(N')}(k)+\sum_{Y=\Sigma^-,\Lambda} U_N^{(Y)}(k) \tag{4}$$

apply to the nucleon single-particle potentials. The nucleons feel therefore direct effects of the other nucleons as well as of the hyperons in the environment, whereas for the hyperons there are only nucleonic contributions, because of the missing hyperon-hyperon potentials.

Equations (1)–(4) define the BHF scheme with the continuous choice of the single-particle energies. Due to the occurrence of U_N and U_Y in Eq. (2) they constitute a coupled system that has to be solved in a self-consistent manner. In our previous work [4] those equations were solved for zero hyperon fraction, since we were interested only in their onset density. In the present paper we proceed further and perform calculations for arbitrary nucleon and hyperon concentrations. Therefore the above equations must be solved for several Fermi momenta of the particles involved.

Once the different single-particle potentials are known, the total nonrelativistic baryonic energy density ϵ and the total binding energy per baryon B/A can be evaluated:

$$\frac{B}{A}=\frac{\epsilon}{\rho_n+\rho_p+\rho_{\Sigma^-}+\rho_\Lambda}, \tag{5}$$

$$\epsilon=\sum_{i=n,p,\Sigma^-,\Lambda}\int_0^{k_F^{(i)}}\frac{dk\,k^2}{\pi^2}\left(m_i+\frac{k^2}{2m_i}+\frac{1}{2}U_i(k)\right)=\epsilon_{NN}+\epsilon_{NY} \tag{6}$$

with

$$\epsilon_{NN}=\sum_{N=n,p}\int_0^{k_F^{(N)}}\frac{dk\,k^2}{\pi^2}\left(m_N+\frac{k^2}{2m_N}+\frac{1}{2}[U_N^{(n)}(k)+U_N^{(p)}(k)]\right), \tag{7a}$$

$$\epsilon_{NY}=\sum_{Y=\Sigma^-,\Lambda}\int_0^{k_F^{(Y)}}\frac{dk\,k^2}{\pi^2}\left(m_Y+\frac{k^2}{2m_Y}\right)+\sum_{N=n,p}\int_0^{k_F^{(N)}}\frac{dk\,k^2}{\pi^2}[U_N^{(\Sigma^-)}(k)+U_N^{(\Lambda)}(k)] \tag{7b}$$

$$=\sum_{Y=\Sigma^-,\Lambda}\int_0^{k_F^{(Y)}}\frac{dk\,k^2}{\pi^2}\times\left(m_Y+\frac{k^2}{2m_Y}+[U_Y^{(n)}(k)+U_Y^{(p)}(k)]\right). \tag{7c}$$

Here we have split the energy density into a part due to the action of nucleon-nucleon forces ϵ_{NN} and due to nucleon-hyperon forces ϵ_{NY}. These quantities depend on the total baryon density of the system $\rho=\rho_N+\rho_Y$, $(\rho_N=\rho_n+\rho_p$, $\rho_Y=\rho_{\Sigma^-}+\rho_\Lambda)$, and on the baryon fractions $x_i=\rho_i/\rho$, $i=p,\Sigma^-,\Lambda$. However, due to the fact that the single-particle potentials $U_N^{(n)}$ and $U_N^{(p)}$ depend only indirectly and therefore very weakly on the hyperon partial densities, the energy density ϵ_{NN} depends, to a good approximation, only on the nucleonic partial density and the proton fraction within the nucleonic subsystem: $\epsilon_{NN}=\epsilon_{NN}(\rho_N,x=\rho_p/\rho_N)$, whereas the dependence on the hyperonic partial densities is concentrated in ϵ_{NY}.

This facilitates the determination of the chemical potentials. They are given by

$$\mu_n(\rho,x_p,x_{\Sigma^-},x_\Lambda)=\frac{\partial\epsilon}{\partial\rho_n}\approx\mu_n(\rho_N,x)+U_n^{(\Sigma^-)}(k_F^{(n)})+U_n^{(\Lambda)}(k_F^{(n)}), \tag{8a}$$

$$\mu_p(\rho,x_p,x_{\Sigma^-},x_\Lambda)=\frac{\partial\epsilon}{\partial\rho_p}\approx\mu_p(\rho_N,x)+U_p^{(\Sigma^-)}(k_F^{(p)})+U_p^{(\Lambda)}(k_F^{(p)}), \tag{8b}$$

$$\mu_Y(\rho,x_p,x_{\Sigma^-},x_\Lambda)=\frac{\partial\epsilon}{\partial\rho_Y}\approx m_Y+\frac{k_F^{(Y)2}}{2m_Y}+U_Y^{(n)}(k_F^{(Y)})+U_Y^{(p)}(k_F^{(Y)}), \tag{8c}$$

where Eqs. (7b), (7c) were used in order to arrive at Eqs. (8a)–(8c).

The contributions to the chemical potentials due to ϵ_{NN} are then the same as in the system without hyperons, namely,

$$\mu_n(\rho_N,x)=\frac{\partial\epsilon_{NN}}{\partial\rho_n}=\left(1+\rho_N\frac{\partial}{\partial\rho_N}-x\frac{\partial}{\partial x}\right)\frac{B}{A}\bigg|_{\rho_Y=0}, \tag{9a}$$

$$\mu_p(\rho_N,x)=\frac{\partial\epsilon_{NN}}{\partial\rho_p}=\left(1+\rho_N\frac{\partial}{\partial\rho_N}+(1-x)\frac{\partial}{\partial x}\right)\frac{B}{A}\bigg|_{\rho_Y=0}, \tag{9b}$$

whereas the contributions due to ϵ_{NY} can be expressed by the appropriate components of the single-particle potentials, which represent corrections to the Fermi energy of the different species. This last step amounts to neglecting certain ''rearrangement'' contributions that appear in the exact expressions for the chemical potentials, namely, from Eqs. (7) one obtains

$$\frac{\partial\epsilon_{NY}}{\partial\rho_n}=\sum_{Y=\Sigma^-,\Lambda}\left[U_n^{(Y)}(k_F^{(n)})+\sum_{N=n,p}\int_0^{k_F^{(N)}}\frac{dk\,k^2}{\pi^2}\frac{\partial U_N^{(Y)}(k)}{\partial\rho_n}\right], \tag{10a}$$

$$\frac{\partial\epsilon_{NY}}{\partial\rho_{\Sigma^-}}=m_{\Sigma^-}+\frac{k_F^{(\Sigma^-)2}}{2m_{\Sigma^-}}+U_{\Sigma^-}(k_F^{(\Sigma^-)})+\sum_{Y=\Sigma^-,\Lambda}\sum_{N=n,p}\int_0^{k_F^{(Y)}}\frac{dk\,k^2}{\pi^2}\frac{\partial U_Y^{(N)}(k)}{\partial\rho_{\Sigma^-}}, \tag{10b}$$

and similarly for p and Λ. Here the last terms represent the rearrangement contributions due to the (weak) dependence of $U_N^{(Y)}$ on ρ_n and $U_Y^{(N)}$ on ρ_{Σ^-}. In the following, the rearrangement contributions of ϵ_{NY} will be neglected, while the much more important ϵ_{NN} is treated exactly, as specified in Eq. (9). This simplifies considerably the numerical effort.

This approximate treatment of ϵ_{NY} is justified, apart from the fact that the nucleon-hyperon forces are weaker than the nucleon-nucleon forces, by a peculiarity of the BHF approach [12], where the chemical potential μ of a species is given by

$$\mu=e_F+U_2(k_F)+\cdots. \tag{11}$$

Here $e_F=k_F^2/2m+U(k_F)$ is the Fermi energy, as determined from the BHF single-particle potential and U_2 is the leading (of second order in the hole line expansion) rearrangement contribution to the single-particle potential, which is given by a diagram representing the conversion of a hole state into a particle state. It therefore vanishes in pure neutron matter for all species different from the neutron, in particular for the proton and the hyperons. For the neutron itself, it was shown

in Ref. [13] that in pure neutron matter the second order rearrangement contribution is rather small, due to the relatively weak neutron-neutron interaction. Therefore, in neutron matter with not too large proton and hyperon fractions, the hyperon chemical potentials and the corrections to the nucleon chemical potentials are well approximated by the respective Fermi energies.

As a further simplification we use the fact that in the so-called parabolic approximation [14], the binding energy per baryon in asymmetric (hyperon-free) nuclear matter depends, to a good approximation, quadratically on the asymmetry parameter $\beta=1-2x$

$$\frac{B}{A}(\rho_N,\beta)\approx\frac{B}{A}(\rho_N,\beta=0)+\beta^2 E_{\rm sym}(\rho_N), \tag{12}$$

where the symmetry energy $E_{\rm sym}$ can be expressed in terms of the difference of the energy per particle between pure neutron ($\beta=1$) and symmetric ($\beta=0$) matter

$$E_{\rm sym}(\rho_N)=\frac{B}{A}(\rho_N,\beta=1)-\frac{B}{A}(\rho_N,\beta=0)$$
$$=\frac{1}{2}\frac{\partial(B/A)}{\partial\beta}(\rho_N,\beta=1). \tag{13}$$

The composition of neutron star matter is crucially dependent on the nuclear symmetry energy. This quantity strongly affects the onset of hyperon formation, as well as other processes such as the neutron star cooling rates [15]. In the parabolic approximation one obtains for the nucleon chemical potentials

$$\mu_{p,n}(\rho_N,\beta)=\mu_{p,n}(\rho_N,0)-\left(\beta^2\pm 2\beta-\beta^2\rho_N\frac{\partial}{\partial\rho_N}\right)E_{\rm sym}(\rho_N) \tag{14}$$

($+$ for p, $-$ for n), and in particular

$$[\mu_n-\mu_p](\rho_N,\beta)=4\beta E_{\rm sym}(\rho_N). \tag{15}$$

As far as the hyperon chemical potentials, Eq. (8c), are concerned, in practice an effective mass approximation can be employed:

$$\mu_Y\approx m_Y+U_Y^0+\frac{(3\pi^2\rho_Y)^{2/3}}{2m_Y^*}, \tag{16}$$

where the ''mean field'' $U_Y^0=U_Y(k=0)$ and the global effective mass

$$\frac{m^\star}{m}=\left[1+\frac{U(k_F)-U(0)}{k_F^2/2m}\right]^{-1} \tag{17}$$

depend on the variables (ρ, x_p, x_{Σ^-}, x_Λ). While U_Y^0 depends sizably on all variables, in practice rather good fits to the calculated single-particle spectra were obtained by taking into account only the ρ_N dependence of m^*/m. Similarly, the corrections to the nucleon Fermi energies appearing in Eqs. (8a), (8b) were found to depend only weakly on the proton fraction x, and parametrized as function of ρ_N and x_Y.

Once the chemical potentials of all species are known, one can proceed to calculate the composition of stellar matter. At high density this is essentially constrained by three conditions: (i) chemical equilibrium among the different species, (ii) charge neutrality, and (iii) baryon number conservation. The chemical potentials are the fundamental input for solving the equations for the chemical equilibrium. At density $\rho\approx\rho_0$ we assume stellar matter composed of a mixture of neutrons, protons, electrons, and muons in β equilibrium [electrons are ultrarelativistic at these densities, $\mu_e=(3\pi^2\rho x_e)^{1/3}$]. In that case the equations read

$$\mu_n=\mu_p+\mu_e, \tag{18}$$

$$\mu_e=\mu_\mu. \tag{19}$$

Since we are looking at neutron stars after neutrinos have escaped, we set the neutrino chemical potential equal to zero. Strange baryons appear at density $\rho\approx(2-3)\rho_0$ [4], mainly in baryonic processes such as $n+n\to p+\Sigma^-$ and $n+n\to n+\Lambda$. The equilibrium conditions for those processes read

$$2\mu_n=\mu_p+\mu_{\Sigma^-}, \tag{20}$$

$$\mu_n=\mu_\Lambda. \tag{21}$$

Further, two conditions of charge neutrality and baryon number conservation allow the unique solution of a closed system of equations, yielding the equilibrium fractions of the baryon and lepton species for each fixed baryon density. They read

$$\rho_p=\rho_e+\rho_\mu+\rho_{\Sigma^-}, \tag{22}$$

$$\rho=\rho_n+\rho_p+\rho_{\Sigma^-}+\rho_\Lambda. \tag{23}$$

Finally, from the knowledge of the equilibrium composition one determines the baryonic equation of state, i.e., the relation between baryonic pressure P_B and baryon density ρ. It can be easily obtained from the thermodynamical relation

$$P_B=\rho^2\frac{d(\epsilon/\rho)}{d\rho}. \tag{24}$$

The total pressure P and the total mass-energy density $\mathcal{E}$ are then calculated by just adding the lepton contributions that are well known from textbooks, see, e.g., Ref. [1]:

$$P=P_B+P_l, \tag{25}$$

$$\mathcal{E}=\epsilon+\epsilon_l. \tag{26}$$

III. RESULTS AND DISCUSSION

A. Single-particle potentials

In order to illustrate some statements made in the previous section, we show in Fig. 1 a representative plot of the single-particle potentials of the different baryons at fixed neutron and proton densities, given by $\rho_N=0.4$ fm^{-3} and

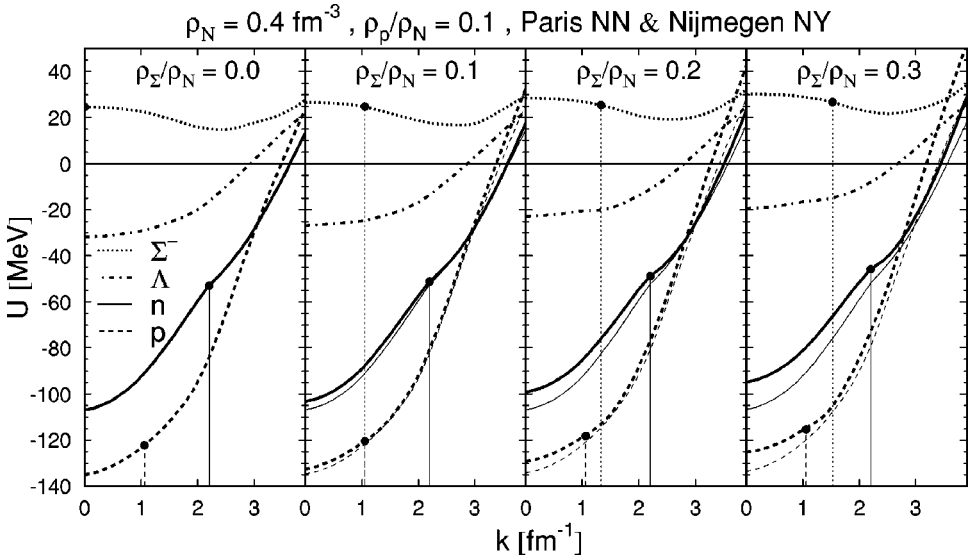

FIG. 1. The single-particle potentials of nucleons n, p and hyperons Σ^-, Λ in baryonic matter of fixed nucleonic density $\rho_N = 0.4\,\mathrm{fm}^{-3}$, proton density $\rho_p/\rho_N = 0.1$, and varying Σ^- density $\rho_{\Sigma^-}/\rho_N = 0.0,\ 0.1,\ 0.2,\ 0.3$. The vertical lines represent the corresponding Fermi momenta of n, p, and Σ^-. For the nucleonic curves, the thick lines represent the complete single-particle potentials U_N, whereas the thin lines show the values excluding the Σ^- contribution, i.e., $U_N^{(n)} + U_N^{(p)}$.

$\rho_p/\rho_N = 0.1$, and varying Σ^- density. Under these conditions the Σ^- single-particle potential is sizably repulsive, while U_Λ is still attractive (see also Ref. [4]) and the nucleons are much stronger bound. The Σ^- single-particle potential has a particular shape with an effective mass m^*/m slightly larger than 1, whereas the lambda effective mass is typically about 0.8 and the nucleon effective masses are much smaller.

The influence of increasing Σ^- density on the hyperonic single-particle potentials is only indirect (since there is no hyperon-hyperon interaction) and therefore rather small. There is some additional repulsion for the nucleons due to the repulsive effective $N\Sigma^-$ interaction, growing with Σ^- partial density. However, these effects represent small variations of the single-particle potentials observed in the hyperon-free system, which justifies the approximate treatment presented in the previous section.

The same principal conclusion applies also to Fig. 2, that displays the same information as Fig. 1, but at higher densities $\rho_N = 0.8\ \mathrm{fm}^{-3}$ and $\rho_p/\rho_N = 0.2$. The main quantitative difference is the fact that under these conditions both hyperon single-particle potentials are quite repulsive.

The results displayed were obtained with the Paris nucleon-nucleon potential. With the Argonne v_{18} one observes only very slight quantitative changes and the corresponding plots are not shown.

B. Stellar matter composition and equation of state

We come now to the presentation of our results regarding neutron stars. In Fig. 3 we show the star composition obtained when the Paris (solid line) or the Argonne v_{18} (dotted line) potential is adopted as nucleon-nucleon force. Three cases are examined, respectively, (a) no hyperons are present, (b) hyperons are free, and (c) hyperons are interacting with nucleons. In panel (a) we show the particle fractions versus the baryon density for matter containing only nucleons and leptons, ignoring hyperons. We note that neutrons are the most dominant species up to very high values of the baryonic density. Electrons and muons are present as well. These general features are common to many models. How-

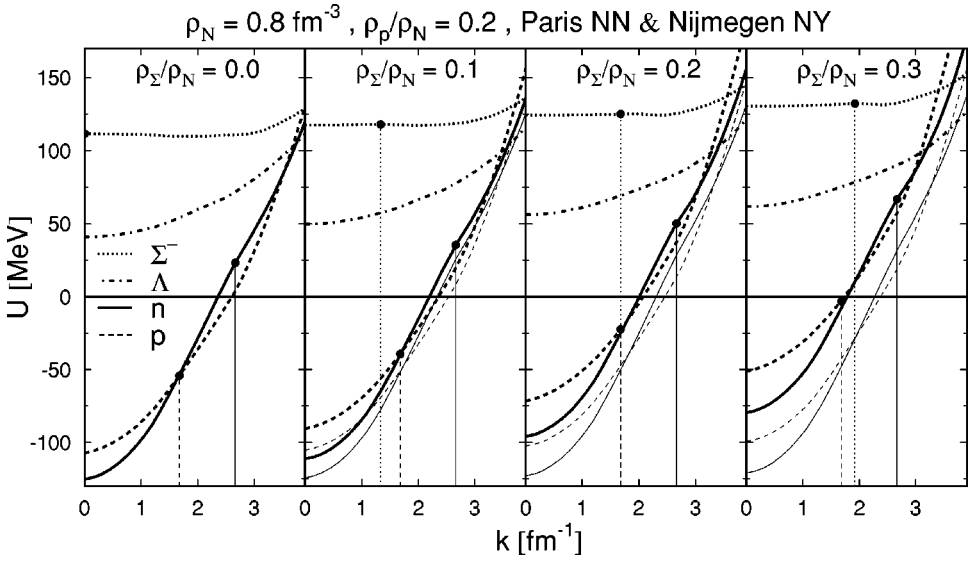

FIG. 2. Same as Fig. 1, but for $\rho_N = 0.8\ \mathrm{fm}^{-3}$ and $\rho_p/\rho_N = 0.2$.

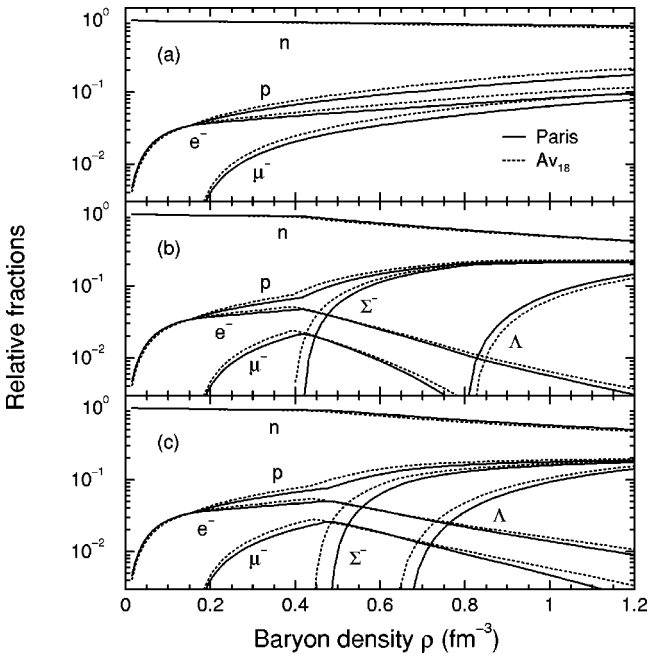

FIG. 3. Composition of neutron star matter in the BHF model. The top panel (a) shows the results without hyperons, the middle panel (b) results with noninteracting hyperons, and the lower panel (c) includes interaction between nucleons and hyperons.

ever, the value of the proton fraction is model dependent, and it affects strongly the direct Urca cooling rates [15].

The picture changes when hyperons are taken into account. This is shown in panels (b) and (c). The Σ^- is the first hyperon to appear, due to its negative charge, whereas Λ formation takes place at higher density. Other hyperon species do not appear in our model. In the free hyperon case [panel (b)], the formation of Σ^- starts at about $\rho \approx 0.4$ fm^{-3}, as was published in our previous paper [4]. In that paper the Λ onset point was approximate, because for its precise determination all the chemical potentials at finite Σ^- fraction are needed. This is performed in the present calculations, and now we estimate exactly the Λ onset point, which is located at about $\rho \approx 0.82$ fm^{-3}. As is clearly shown, the thresholds for hyperon formation are weakly dependent on the two-body force. The hyperon fractions are substantial at high density and constitute a large portion of the stellar core matter. The appearance of hyperons induces a deleptonization of the baryonic medium, mainly because of the charge neutrality condition. Leptons disappear at high baryonic density, thus hindering formation of kaon condensate [16].

When the nucleon-hyperon interaction is taken into account, the scenario described above changes quantitatively. In fact, since the Σ^- Fermi energy is repulsive starting from densities just above normal nuclear matter density [4], the onset point is shifted to slightly higher density. On the contrary, the Λ formation starts at density lower than in the free case because the Λ Fermi energy is attractive over a wide range of densities. This is clearly shown in panel (c). However, the hyperon population is smaller than in the free case and deleptonization is less drastic, because the repulsive core of the *NY* interactions becomes relevant at high density. However, even in this case, kaon condensation cannot occur. Again, we note how those results are slightly dependent on the two-body interaction.

The main consequence of introducing additional particle species into matter is the softening of the EOS. This softening is essentially due to the conversion of kinetic energy of the already present species into masses of the new species. The decrease of the lepton population does add further softening, but this effect is quite small. The nature of the EOS is thus dependent on the number of species, as well as on the details of the strong interaction. It can be instructive to begin with the equation of state corresponding to the case (a), i.e., when no hyperons are present. This is displayed in Fig. 4 (solid line). On the left (right) hand side we show the equation of state obtained when the Paris (Av_{18}) potential is adopted as nucleon-nucleon interaction. That calculation has been improved with respect to the one published in Ref. [7], since more channels are now taken into account in the solution of the Bethe-Goldstone equation. This has produced a better convergence of the iterative procedure for high values of nuclear matter density.

The properties of the EOS change when hyperons are taken into account. In particular, the dotted line corresponds

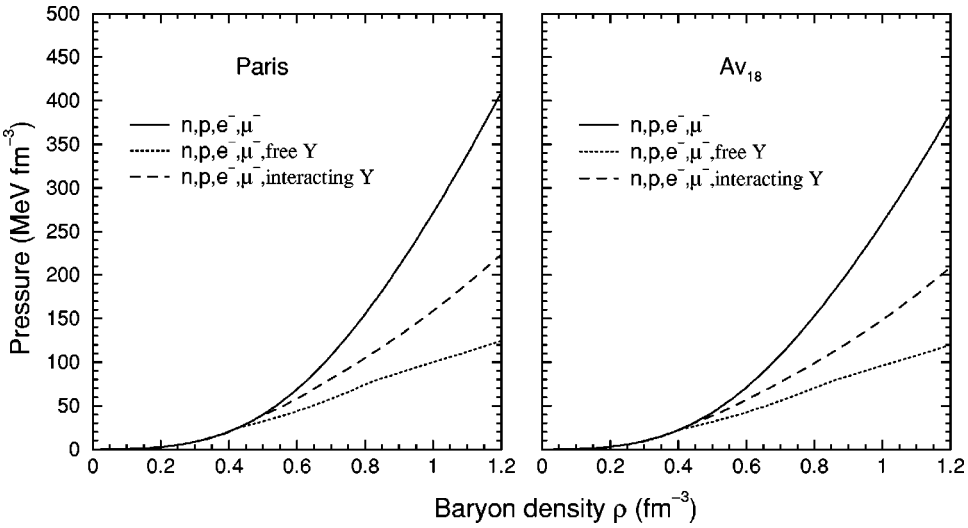

FIG. 4. EOS of neutron star matter in the BHF model. Results without hyperons (solid lines), with free hyperons (dotted lines), and with interacting hyperons (dashed lines) are shown. The Paris (left) or Argonne v_{18} (right) nucleon-nucleon potentials were used.

to the case of nuclear matter containing leptons and free hyperons. The presence of hyperons induces a strong softening of the equation of state. The inclusion of the nucleon-hyperon interaction produces an equation of state stiffer than in the free hyperon case. This is shown by the dashed line. We observe a similar behavior when the Argonne v_{18} potential is used.

However, it is well known that nonrelativistic calculations, based on purely two-body interactions, fail to reproduce the correct saturation point of symmetric nuclear matter [17]. This deficiency is commonly corrected by introducing three-body forces (TBFs) among nucleons. This changes the scenario described above. Our method of treating TBFs is discussed in the following paragraph.

C. Inclusion of three-body forces

It is commonly known that a complete theory of three-body forces is not available so far. Therefore one has to work with phenomenological approaches. A realistic model for nuclear TBFs is the so-called Urbana model [18], which consists of an attractive term due to two-pion exchange with excitation of an intermediate Δ resonance, and a repulsive phenomenological central term. We introduced the same Urbana three-nucleon model within the BHF approach (for more details see Ref. [7]). In our approach the TBF is reduced to a density dependent two-body force by averaging on the position of the third particle, assuming that the probability of having two particles at a given distance is reduced according to the two-body correlation function. The corresponding EOS satisfies several requirements, namely, (i) it reproduces correctly the nuclear matter saturation point [7], (ii) the incompressibility is compatible with values extracted from phenomenology [19], (iii) the symmetry energy is compatible with nuclear phenomenology, (iv) the causality condition is always fulfilled.

Figure 5 shows the values of the symmetry energy for the different EOSs that we consider, namely, the nonrelativistic Brueckner calculations with the Paris and the Argonne v_{18} potentials with and without three-body forces. For comparison, we report also the symmetry energy of a recent calculation performed with a Dirac-Brueckner (DBHF) model [20], but with the Bonn-*A* potential. We should remind the reader that the DBHF treatment is equivalent [21] to introducing in the nonrelativistic BHF the three-body force corresponding to the excitation of a nucleon-antinucleon pair, the so-called *Z* diagram [22], which is repulsive at all densities. We therefore expect that the symmetry energy calculated within the DBHF approach is always larger than the one obtained in the nonrelativistic BHF calculation, without and with three-body force, since in the last case both an attractive and a repulsive component is introduced. From Fig. 5 we see that this is true for all the potentials discussed in this paper, except for the Argonne v_{18} potential with TBFs, maybe because of its strongly repulsive core. On the contrary, in the low density region ($\rho \lesssim 0.3$ fm^{-3}), both BHF +TBF symmetry energies and DBHF calculations are very similar.

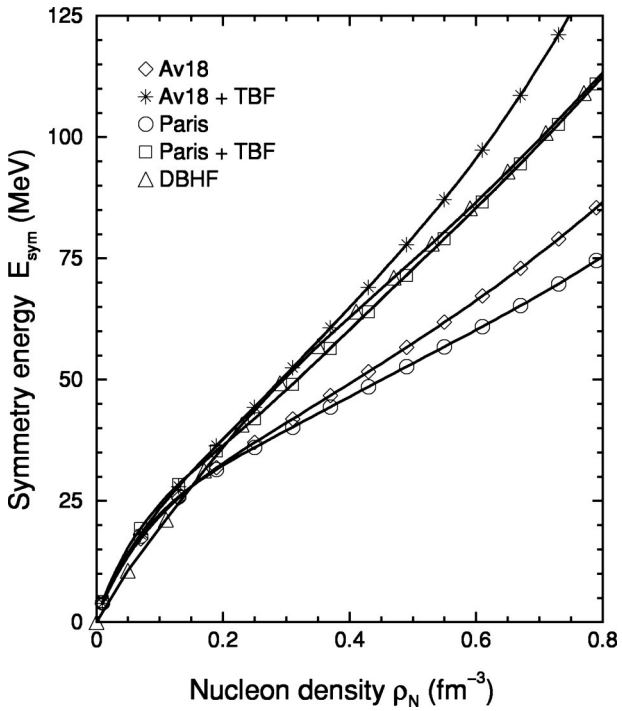

FIG. 5. Nucleonic symmetry energy as a function of nucleon density obtained in different theoretical models of nuclear matter.

We can proceed now to the discussion of the nuclear matter composition when TBFs are included in the equation of state. Please note that TBFs are included only for nucleons. Hyperons interact via two-body forces with nucleons (we adopt the Nijmegen soft-core potential, as discussed in the Introduction), and do not interact at all among themselves. Since no experimentally tested hyperon-hyperon potentials are currently available, this assumption is in line with the exploratory character of this work. Of course, their eventual introduction may change the scenarios resulting from our analysis.

In Fig. 6 we show the matter composition when the TBFs among nucleons is included in the BHF calculation. The notation is the same as in Fig. 3, i.e., the solid line represents the composition obtained with the Paris+TBF potential, whereas the dotted line corresponds to the composition obtained with the Argonne Av_{18} potential. Let us first discuss the case without hyperons, displayed in panel (a). Because of its repulsive character at high densities, the higher value of the symmetry energy allows more easily the conversion of neutrons into protons and leptons compared to the case without TBFs. The proton fraction can now exceed the ''critical'' value $x_{\mathrm{Urca}} \approx (11-15)$ % needed for the occurrence of direct Urca processes [15].

The chemical composition of nuclear matter changes completely when hyperons are taken into account. In panel (b) we show the particle fractions obtained when the hyperons are free. We notice that the three-body forces shift the onset points of both Σ^- and Λ, as previously published [4], down to densities 2–3.5 times normal nuclear matter density. Deleptonization takes place, and leptons disappear almost completely just after hyperon formation, because now it is

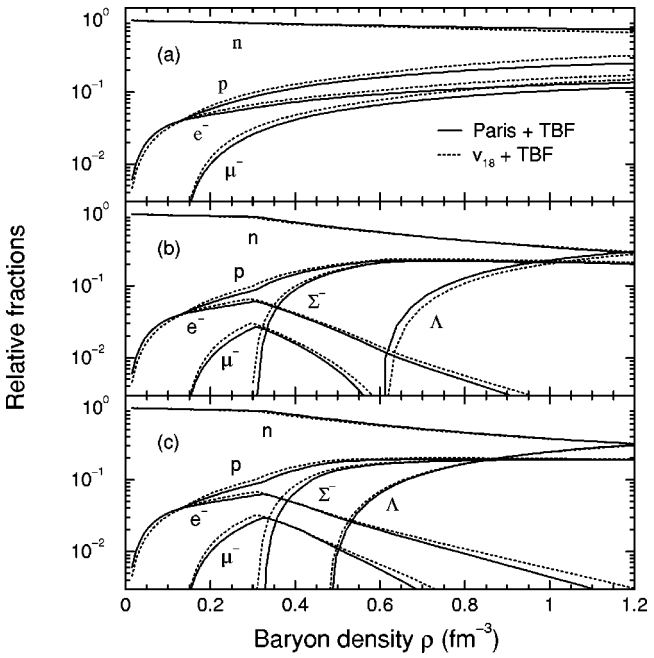

FIG. 6. As in Fig. 3, but the nucleon-nucleon potentials are supplemented by three-body forces.

more convenient energetically to maintain the charge neutrality through Σ^- formation than β decay. At high density nucleons and hyperons are present almost in the same percentage.

This scenario does not change qualitatively when the nucleon-hyperon interaction is included, see panel (c). The main difference is that the hyperon onset points move again, respectively, to higher (lower) density because of the repulsive (attractive) character of the Σ^- (Λ) Fermi energy at those densities. Even in this case the stellar core is composed by an almost equal fraction of nucleons and hyperons. Once again those compositions look very much the same both with the Paris and the Av_{18} potential.

The corresponding equations of state obtained when TBFs are added to the two-body forces are listed in Table I and shown in Fig. 7. On the left (right) hand side we show our results obtained with the Paris (Av_{18}) potential plus TBFs. The solid line shows the equation of state of asymmetric β-stable matter with a percentage of electrons and muons. It looks much stiffer than the case when hyperons are introduced. The dotted line represents the equation of state of nuclear matter containing free hyperons, whereas the dashed line corresponds to the case of hyperons interacting with the nucleonic medium. If we compare the equations of state obtained without and with TBFs, i.e., the dashed lines of Figs. 4 and 7, we see only a small difference. This can be understood by looking at the final compositions, respectively, panels (c) of Figs. 3 and 6. There we note that the net effect of TBFs is a decreased presence of neutrons and an enhanced population of Λ, whereas protons and Σ^- are only slightly affected by TBFs, keeping the total percentage of neutral charge almost the same in both cases. Therefore, as far as the equation of state is concerned, we expect that the relation between pressure and baryon density is very similar without and with TBFs. This is indeed the case and means that hyperon formation is a mechanism for pressure control, as already found by the authors of Ref. [23] within a phenomenological approach.

TABLE I. EOS for β-stable matter with hyperons obtained in the BHF approximation using the Argonne v_{18} or Paris two-body interaction complemented by the Urbana model for three-body forces. We display the baryon density ρ, the total mass density $\mathcal{E}$, and the total pressure P.

ρ (fm^{-3})	$\mathcal{E}$ (10^{14} g cm^{-3})		P(10^{34} dyn cm^{-2})	
	Av_{18}+TBF	Paris+TBF	Av_{18}+TBF	Paris+TBF
0.08	1.27	1.27	0.07	0.06
0.16	2.64	2.63	0.42	0.39
0.2	3.33	3.33	0.80	0.75
0.3	5.13	5.12	2.62	2.52
0.4	7.11	7.20	4.70	5.05
0.5	9.01	8.96	7.16	7.40
0.6	11.1	11.0	9.71	10.1
0.7	13.0	13.1	12.2	12.8
0.8	15.3	15.2	15.3	16.2
0.9	17.3	17.2	18.3	18.9
1.0	20.0	20.1	22.5	23.5
1.1	21.8	22.1	25.7	27.2
1.2	23.9	24.4	29.3	30.5
1.3	26.0	26.2	33.3	34.5
1.4	28.8	28.5	38.8	39.2
1.5	31.1	31.1	43.7	45.2
1.6	33.5	33.4	49.0	49.7
1.7	35.4	36.2	53.2	56.2

Finally, we comment on the deleptonization of the baryonic matter. This is clearly indicated by the chemical potentials, drawn in Fig. 8. In panel (a) we display the chemical potentials for neutrons and protons obtained with the Paris potential supplemented by TBFs (the value of the neutron mass has been subtracted), whereas in panel (b) the electron chemical potential is shown. We observe a monotonously increasing function of the baryon density when no hyperons are present (dashed lines), whereas the appearance of negatively charged hyperons interacting with the medium (solid line) induces a strong deleptonization of the matter. Thus the formation of hyperons and the consequent deleptonization will suppress meson condensation [24,25]. Although kaon and antikaon condensation has been proposed as possible state of matter inside neutron stars [16], also recent investigations within the relativistic mean field approach [25] find the onset of kaon condensation quite unlikely. In any case, the importance of meson condensation will be strongly diminished by allowing for the dominant hyperon formation.

D. Neutron stars

As already discussed in the Introduction, the knowledge of the equation of state is essential in order to build models of both static and rotating neutron stars. In fact, the EOS for β-stable matter can be used in the Tolman-Oppenheimer-Volkoff (TOV) equations [26,27] to compute the neutron star

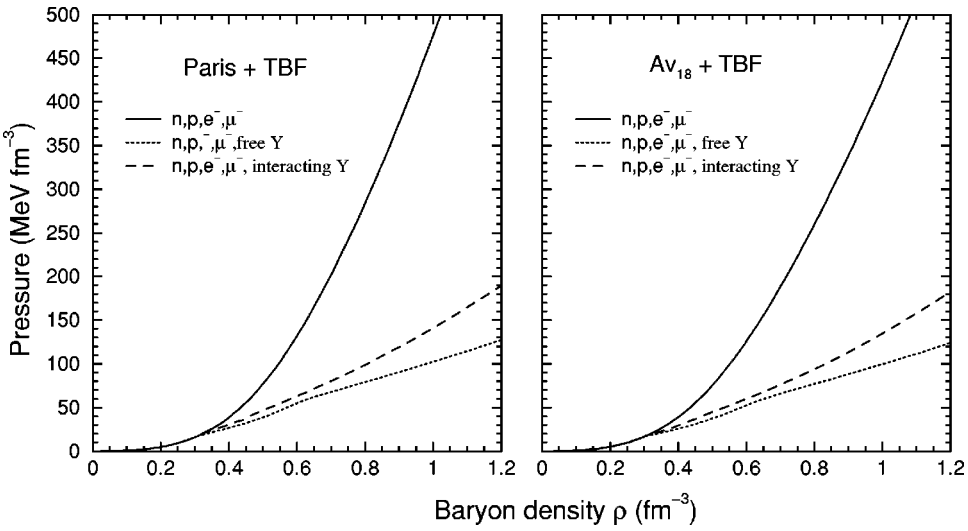

FIG. 7. As in Fig. 4, but including three-body forces.

mass and radius as a function of the central density. As a first step, we neglect the effects of rotations and calculate the mass-radius relation assuming that a neutron star is a spherically symmetric object in hydrostatic equilibrium. Then the equilibrium configurations are simply obtained by solving the TOV equations for the total pressure P and the enclosed mass m,

$$\frac{dP(r)}{dr} = -\frac{Gm(r)\mathcal{E}(r)}{r^2}\frac{\left[1+\frac{P(r)}{\mathcal{E}(r)}\right]\left[1+\frac{4\pi r^3 P(r)}{m(r)}\right]}{1-\frac{2Gm(r)}{r}}, \tag{27}$$

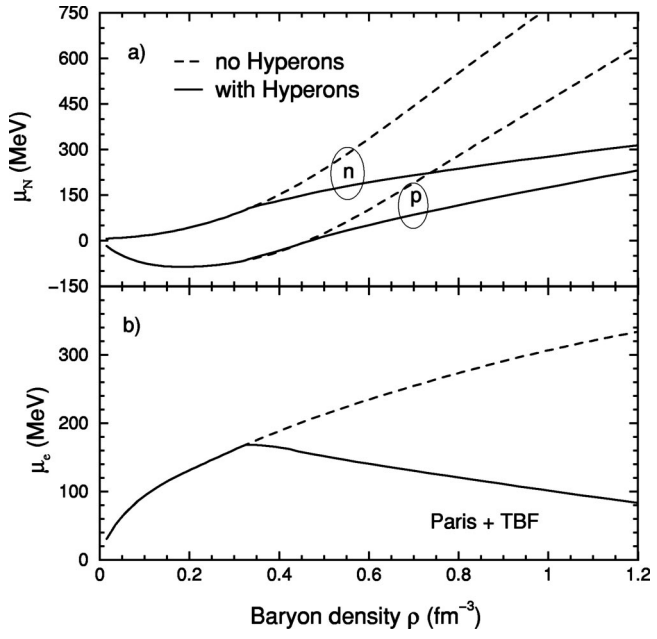

FIG. 8. Chemical potentials of the different species as a function of baryon density in neutron star matter. The upper panel (a) shows results for neutrons and protons, whereas the electron chemical potential is displayed in panel (b). The dashed (solid) line denotes the case of matter composition without (with) interacting hyperons.

$$\frac{dm(r)}{dr} = 4\pi r^2 \mathcal{E}(r), \tag{28}$$

G being the gravitational constant (we assume $c=1$). Starting with a central mass density $\mathcal{E}(r=0)\equiv\mathcal{E}_c$, we integrate out until the pressure on the surface equals the one corresponding to the density of iron. This gives the stellar radius R and the gravitational mass is then

$$M_G \equiv m(R) = 4\pi \int_0^R dr\, r^2 \mathcal{E}(r). \tag{29}$$

For the outer part of the neutron star we have used the equations of state by Feynman-Metropolis-Teller [28] and Baym-Pethick-Sutherland [29], and for the middle-density regime ($0.001\ \text{fm}^{-3} < \rho < 0.08\ \text{fm}^{-3}$) we use the results of Negele and Vautherin [30]. In the high-density part ($\rho > 0.08\ \text{fm}^{-3}$) we use alternatively the equations of state displayed in Table I. For comparison, we also perform calculations of neutron star structure for the case of purely nucleonic asymmetric and β-stable matter with some lepton fraction.

The results are plotted in Fig. 9, where we display the gravitational mass M_G (in units of the solar mass $M_\odot$) as a function of the radius R and the central baryon density ρ_c. We report the results obtained using either the Av_{18} or the Paris two-body potential with three-body forces. The solid lines represent the equilibrium configurations of neutron stars composed only of nucleons and leptons; the dashed lines show the configurations of stars whose composition includes interacting hyperons. As we can see, the softening of the equation of state due to the presence of additional baryonic species produces a strong decrease in the value of the limiting mass, from about $2M_\odot$ down to $1.2M_\odot$, almost independent on the nucleon-nucleon interaction. The limiting central densities stay nearly constant at about 7 times normal nuclear matter density.

For clarity we report in Table II the properties of the maximum mass configuration obtained with equations of state of β-stable asymmetric nuclear matter with and without hyperons. Without hyperons we observe mainly the effect of

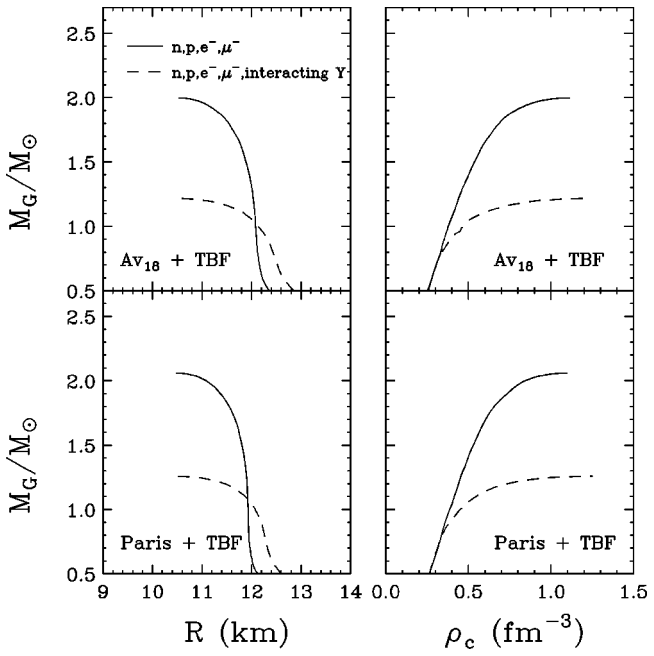

FIG. 9. Neutron star mass as a function of radius (left) or central baryon density (right) in the BHF+TBF model. Results without (solid lines) and with (dashed lines) interacting hyperons are compared.

three-body forces among nucleons on the equation of state and, therefore, on the values of the maximum mass configuration. In particular, the increased repulsion among nucleons produces a stiffer equation of state and a higher value of the maximum mass, with a smaller radius and central density. Even in this case we note a strong similarity in the limiting values independently on the two-body potential.

The situation changes dramatically when interacting hyperons are included. In this case the additional repulsion produced by the nucleon three-body forces is counterbalanced by the increased population of hyperons, thus leading to a very soft equation of state. The values of the maximum mass do not differ very much from those calculated without TBFs. However, the values of the maximum central densities are substantially different, despite the EOS looking similar in the two cases. When TBFs are included, this value becomes smaller, see Table II. Without TBFs, in fact, the EOS is slightly stiffer at higher densities and the corresponding curve of the mass vs central density (not reported in Fig. 9)

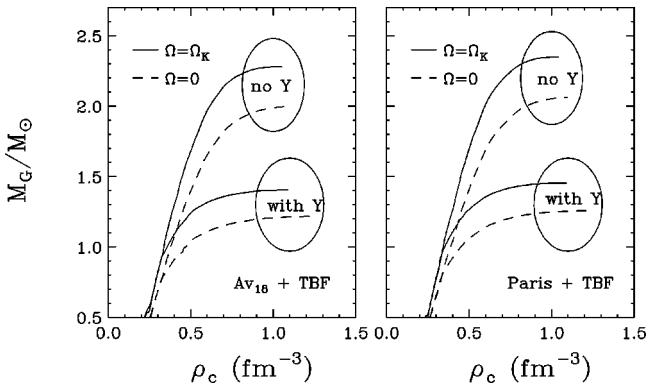

FIG. 10. Neutron star mass as a function of central baryon density in the BHF+TBF model with and without hyperons. Curves for nonrotating stars (dashed lines) and rotations at the Kepler frequency (solid lines) are shown.

has a shallow maximum at larger central density. However, the corresponding maximum mass is only slightly larger than in the case with TBFs, as reported in Table II. This also shows the sensitivity of the results on the details of the nuclear EOS. It has to be noticed that, for stable configurations, at a given value of the neutron star mass the central density is larger when TBFs are included. Furthermore, neutron stars built with equations of state of matter containing baryons interacting via TBFs possess a core with a larger hyperon population than in the case without TBFs.

The above scenario changes when the rotations are included. In particular, in order to treat stellar rotations in general relativity, we follow the method discussed in Ref. [10]. In those papers the Einstein equations for rotating massive objects are solved perturbatively with a modified version of Hartle's method. With this method the authors are able to determine sequences of star models rotating at their respective general relativistic Kepler frequency Ω_K. In Fig. 10 we display the net effect of rotations on the mass-density relation. There we display star sequences at equilibrium both for static (dashed lines) and rotating (solid lines) neutron stars. The upper curves refer to equations of state without hyperons, whereas the lower curves refer to equations of state containing hyperons. The rotations increase the value of the limiting mass by about 12%, decreasing the limiting value of the central density. Again, we do not observe a significant difference for the various NN potentials. In Table II we report also the values of the limiting configuration.

TABLE II. Properties of the maximum mass configuration obtained for different equations of state: M_G is the gravitational (maximum) mass, R is the corresponding radius, and ρ_c the central baryon density. In each case the results of the EOS without hyperons (no Y), including hyperons (Y), and including rotation at the Kepler frequency (Y+Rot) are listed.

EOS	$M_G/M_\odot$			R (km)			ρ_c (fm^{-3})		
	no Y	Y	Y+Rot	no Y	Y	Y+Rot	no Y	Y	Y+Rot
Av_{18}	1.64	1.26	1.44	9.10	8.70	10.53	1.53	1.86	1.56
Paris	1.67	1.31	1.50	8.90	8.62	10.30	1.59	1.84	1.62
Av_{18}+TBF	2.00	1.22	1.41	10.54	10.46	12.68	1.11	1.25	1.09
Paris+TBF	2.06	1.26	1.45	10.50	10.46	12.65	1.10	1.25	1.09

IV. CONCLUSIONS

The principal finding of this paper has been a surprisingly low value for the maximum mass of a ''neutron star'' that barely comprises the ''canonical'' value $M \approx 1.4 M_{\odot}$. While certainly the technical insufficiencies and approximations of our approach can account for an uncertainty on this limit of a few percent, it seems rather difficult theoretically to avoid a rather low limit on the maximum mass. As we have seen, the mere presence of additional baryonic degrees of freedom in the form of hyperons renders the maximum mass quite insensitive to the stiffness of the *nucleonic* equation of state. Because the hyperonic onset densities at about 2–3 times normal density seem to be rather robust and model independent, it seems that the maximum mass can be substantially increased only if the nucleon-hyperon and/or hyperon-hyperon effective interactions become extremely repulsive at high density. Unfortunately at present the experimental information on the nucleon-hyperon interaction is rather scarce, and for the hyperon-hyperon case practically nonexistent.

Nevertheless, recently the Nijmegen *NY* potential model was extended to the full *YY* case by imposing isospin symmetry [31]. In Ref. [32] these new potentials have been used to include the hyperon-hyperon interaction in neutron star studies within a similar approach, using a variational nucleonic EOS together with hyperon single-particle potentials determined in a standard choice Brueckner scheme. The obtained maximum neutron star masses turn out to be quite similar to the ones presented in this work.

Let us also mention that, within different versions of the relativistic mean field theory, the introduction of hyperons in the EOS of nuclear matter leads to maximum masses that are only slightly larger [33] or substantially larger [34] than the ones reported here. This illustrates the lack of constraints imposed on this type of models.

In Ref. [34] the possible onset of quark-gluon plasma in the interior of neutron stars is also investigated and found to be unlikely to occur up to baryon densities we found in the interior of the neutron star. It is expected that the possible presence of the deconfined phase would produce an additional softening of the EOS, and therefore a further decrease of the critical mass.

It seems, therefore, that indeed the theoretical limit of the maximum mass of a neutron star is rather small. A lowering of the maximum mass of neutron stars due to the onset of hyperon formation was actually already qualitatively anticipated in the very first articles which investigated baryonic matter with hyperons [35]. However, no quantitative analysis could be done at that time, due to the uncertainties in the theoretical models. Within the present microscopic approach we can give now a more quantitative prediction of this effect.

ACKNOWLEDGMENTS

We warmly thank F. Weber, who provided us with his code for the calculation of the structure of rotating neutron stars and acknowledge useful discussions with A. Polls and A. Ramos. This work was supported in part by the program ''Estancias de científicos y tecnólogos extranjeros en España.''

[1] S. L. Shapiro and S. A. Teukolsky, *Black Holes, White Dwarfs and Neutron Stars* (Wiley, New York, 1983); N. K. Glendenning, *Compact Stars* (Springer, New York, 1997).

[2] S. E. Thorsett and D. Chakrabarty, Astrophys. J. **512**, 288 (1999).

[3] E. Witten, Phys. Rev. D **30**, 272 (1984); G. Baym, E. W. Kolb, L. McLerran, T. P. Walker, and R. L. Jaffe, Phys. Lett. B **160**, 181 (1985); N. K. Glendenning, Mod. Phys. Lett. A **5**, 2197 (1990).

[4] M. Baldo, G. F. Burgio, and H.-J. Schulze, Phys. Rev. C **58**, 3688 (1998).

[5] M. Lacombe, B. Loiseau, J. M. Richard, R. Vinh Mau, J. Côté, P. Pirès, and R. de Tourreil, Phys. Rev. C **21**, 861 (1980).

[6] R. B. Wiringa, R. A. Smith, and T. L. Ainsworth, Phys. Rev. C **29**, 1207 (1984).

[7] M. Baldo, I. Bombaci, and G. F. Burgio, Astron. Astrophys. **328**, 274 (1997).

[8] P. Maessen, Th. Rijken, and J. de Swart, Phys. Rev. C **40**, 2226 (1989).

[9] R. B. Wiringa, V. G. J. Stoks, and R. Schiavilla, Phys. Rev. C **51**, 38 (1995).

[10] F. Weber and N. K. Glendenning, Phys. Lett. B **265**, 1 (1991); F. Weber and N. K. Glendenning, Astrophys. J. **390**, 541 (1992).

[11] H.-J. Schulze, A. Lejeune, J. Cugnon, M. Baldo, and U. Lombardo, Phys. Lett. B **355**, 21 (1995); Phys. Rev. C **57**, 704 (1998).

[12] K. A. Brueckner and J. L. Gammel, Phys. Rev. **109**, 1023 (1958); J.-P. Jeukenne, A. Lejeune, and C. Mahaux, Phys. Rep., Phys. Lett. **25C**, 83 (1976); M. Baldo, I. Bombaci, G. Giansiracusa, U. Lombardo, C. Mahaux, and R. Sartor, Phys. Rev. C **41**, 1748 (1990).

[13] W. Zuo, G. Giansiracusa, U. Lombardo, N. Sandulescu, and H.-J. Schulze, Phys. Lett. B **421**, 1 (1998).

[14] A. Lejeune, P. Grangé, M. Martzolff, and J. Cugnon, Nucl. Phys. **A453**, 189 (1986); I. Bombaci and U. Lombardo, Phys. Rev. C **44**, 1892 (1991); W. Zuo, I. Bombaci, and U. Lombardo, *ibid.* **60**, 024605 (1999).

[15] J. Lattimer, C. Pethick, M. Prakash, and P. Haensel, Phys. Rev. Lett. **66**, 2701 (1991).

[16] V. R. Pandharipande, C. J. Pethick, and V. Thorsson, Phys. Rev. Lett. **75**, 4567 (1995); G. Q. Li, C.-H. Lee, and G. E. Brown, Nucl. Phys. **A625**, 372 (1997).

[17] F. Coester, S. Cohen, B. D. Day, and C. M. Vincent, Phys. Rev. C **1**, 769 (1970).

[18] J. Carlson, V. R. Pandharipande, and R. B. Wiringa, Nucl. Phys. **A401**, 59 (1983); R. Schiavilla, V. R. Pandharipande, and R. B. Wiringa, *ibid.* **A449**, 219 (1986).

[19] W. D. Myers and W. J. Swiatecki, Nucl. Phys. **A601**, 141 (1996).

[20] G. Q. Li, R. Machleidt, and R. Brockmann, Phys. Rev. C **45**, 2782 (1992).
[21] M. Baldo, G. Giansiracusa, U. Lombardo, I. Bombaci, and L. S. Ferreira, Nucl. Phys. **A583**, 599 (1995).
[22] G. E. Brown, W. Weise, G. Baym, and J. Speth, Comments Nucl. Part. Phys. **17**, 39 (1987).
[23] S. Balberg and A. Gal, Nucl. Phys. **A625**, 435 (1997).
[24] P. J. Ellis, R. Knorren, and M. Prakash, Phys. Lett. B **349**, 11 (1995); R. Knorren, M. Prakash, and P. J. Ellis, Phys. Rev. C **52**, 3470 (1995).
[25] J. Schaffner and I. N. Mishustin, Phys. Rev. C **53**, 1416 (1996); J. Schaffner, A. Gal, I. N. Mishustin, H. Stöcker, and W. Greiner, Phys. Lett. B **324**, 268 (1994).
[26] R. C. Tolman, Proc. Natl. Acad. Sci. USA **20**, 3 (1934).
[27] J. Oppenheimer and G. Volkoff, Phys. Rev. **55**, 374 (1939).
[28] R. Feynman, F. Metropolis, and E. Teller, Phys. Rev. **75**, 1561 (1949).
[29] G. Baym, C. Pethick, and D. Sutherland, Astrophys. J. **170**, 299 (1971).
[30] J. W. Negele and D. Vautherin, Nucl. Phys. **A207**, 298 (1973).
[31] Th. A. Rijken, V. G. J. Stoks, and Y. Yamamoto, Phys. Rev. C **59**, 21 (1999); V. G. J. Stoks and Th. A. Rijken, *ibid.* **59**, 3009 (1999).
[32] I. Vidaña, A. Polls, A. Ramos, Ø. Elgarøy, L. Engvik, and M. Hjorth-Jensen, nucl-th/9912016.
[33] S. Pal, M. Hanauke, I. Zakout, H. Stöcker, and W. Greiner, Phys. Rev. C **60**, 015802 (1999).
[34] K. Schertler, S. Leupold, and J. Schaffner-Bielich, Phys. Rev. C **60**, 025801 (1999).
[35] A. G. W. Cameron, Astrophys. J. **130**, 884 (1959); V. R. Pandharipande, Nucl. Phys. **A178**, 123 (1971); H. A. Bethe and M. B. Johnson, *ibid.* **A230**, 1 (1974).